International Journal of Theoretical and Applied Mathematics
2024, Vol. 10, No. 3, pp. 38-50
https://doi.org/10.11648/j.ijtam.20241003.12

Research Article

The Upshots of Dufour and Soret in Stretching Porous Flow of Convective Maxwell Nanofluid with Nonlinear Thermal Emission

Michael Williams*, Isah Bala Yabo

Department of Mathematics, Usmanu Danfodiyo University, Sokoto, Nigeria

Abstract

In this paper, the combined upshot of Soret and Dufoue of a convective Maxwell nanofluid on a porous perpendicular surface with nonlinear thermal emission was investigated. In the present work, the impact of permeable stretching sheet, nonlinear thermal emission, heat sour sink, Dufour and Soret effect, chemical reaction, Brownian motion and thermophoresis in a convective Maxwell nanofluid flow is widely discussed. The governing equations derived for the problem are highly nonlinear coupled partial differential equations. The governing equations were transformed into ordinary differential equations using Lie symmetry group alterations. The BVP4C MATLAB solver was employed to solve the ordinary differential equations numerically after validating the convergence of the method with existing results in the literature. The numerical results were established and discussed using tables and graphs. It was found that variations in porosity parameter (K), Dufour (Du) and Soret (Sr) improves velocity, temperature and concentration profiles respectively and the present of nonlinear thermal radiation and heat source emit more heat for the flow. Also, it is exciting to report that both porosity (K) and Dufour (Du) parameters has a strong impact on the flow of skin frictions, Nusselt number and Sherwood number. However, the current results may present applications in the areas of petroleum reservoir, heat exchangers, steel industries, cooling applications, nuclear waste disposal and so on.

Keywords

Soret, Dufour, Heat Source, and Nonlinear Thermal Radiation

1. Introduction

The attentions of several researchers on the area of combine effect of Soret and Dufour have been drowned due to the recent awakening engineering and scientific applications. It is applicable in the areas of petroleum reservoir, heat exchangers, steel industries, cooling applications, nuclear waste disposal and so on. Soret and Dufour played a vital role in the double-diffusive area. This is because their upshots orders of magnitude are smaller. The product of mass flux situated in mass equation caused by temperature slope is called Soret effect while the product of energy flux located in energy equation instigated by mass gradient is called Dufour effect. Ismail *et al*. [1] established the upshots of thermo-diffusion and diffusion-thermo on a parallel porous plate. It was solved analytically and finite difference method was used to validate their results numerically. However, they noted different parallel flow behaviors due to buoyance ratio- diffusion thermo.

*Corresponding author: michealwilliams185@gmail.com (Michael Williams)

Received: 15 August 2024; **Accepted:** 6 September 2024; **Published:** 18 October 2024

Safae *et al*. [2] dissected the upshot of heat source and thermo diffusion carried out numerically within the stretching sheet. They noted that Soret upshot is increased with the presence of R on the mean concentration and reduced with absent of R. Some analysis of Soret and Dufour effects can be seen in the studies of Bidemi and Ahmad [3], Michael and Isah [4].

The modern exploration in nanotechnology to develop the effectiveness of refined thermal systems was established as a result of novel energy sources. The size of the particles in nanofluid is nanometer which is made by suppressing the particles in a fundamental liquid. Nanofluids have been form by several forms of base fluid and nanoparticles as a means of heat transfer for diverse procedures. The most common base fluids in nanofluids are ethylene glycol, water, and motor engine oil. While water is a renewable resource, it is not ideal due to its low thermal conductivity. On the other hand, motor engine oil and ethylene glycol have high viscosity but are environmentally toxic. Additionally, mixtures of water or ethylene glycol with nanoparticles are commonly used as car coolants to enhance engine performance. Computers of high performance make used of cooling electronic technology to reach an extreme power of 100,300 W/cm^2 in a microprocessor circuit. Rana *et al*. [5] applied Buongiorno model to recommend a non-homogeneous type which identified seven components that influenced the upgrading of warmness modification to Nanofluid, thermophoresis and Brownian motion had been determined to be the extreme contributing components. Madhukesh *et al*. [6] investigated the consequences of the states of the higher temperature variation, thermal emission and viscous heat. In addition, they improved Buongiorno mathematical model with Brownian motion, thermophoresis and gyrotactic microorganisms. Therefore, the quest for the relevant application of nanofluid drives the efforts of many authors in conducting research on the related topic in recent years which include Puneeth [7], Khan [8], Hayat [9], Gireesha [10], Hussain [11] and Isah [12].

Heat and mass transfer over an extended surface is another attractive area of research with applications in many industrial and engineering activities. The prediction of heat and mass transport behaviors in non-Newtonian fluids encompasses applications in thermal engineering, metal spinning, and sphere bed processes, glass fiber, hot rolling, and so on. Zaid *et al* [13] investigated the free convective flow of a viscous material concerning heat and mass transfer in a permeable channel using cubic B-spline collocation outline. Hayat *et al.* [14] studied the flow of Eyring-Powell fluid of heat and mass transfer on a stretching sheet. Mahanthesh *et al*. [15] addressed the heat and mass flow of chemical responses over motionless and moving pattern. Selimefendigil *et al.* [16] investigated the configurations of heat and mass transfer transportation in a fluid flow through the channel pattern. Ahmed *et al*. [17] analyzed the microstructural implications of the finite difference scheme to evaluate the numerical simulations of heat and mass transfer in a viscous liquid.

The nonlinear thermal radiation has attracted the attention of many researchers due to several engineering applications. Though, processing industries make use of nonlinear thermal radiation to produce heat to get a good finished product. The plants for electricity generation, rocket propulsion, turbine for gas and so on are produced from the finished products. Khan *et al*. [18] inspected the significance of nonlinear Rosseland approximation in a Walter-B nanoliquid by utilizing Brownian motion, thermophoresis, and convective boundary conditions. Their results show that an increasing Schmidt number reduces the concentration of the nanofluid. Ilias *et al*. [19] explored the magnetohydrodynamic heat transfer on an extending sheet. Their findings revealed how heat transfer and fluid flow impact the leading surface. Jha and Samaila [20] supported the significance of nonlinear Rosseland approximation and thermophoresis on heat and mass transfer in mixed convective vertical channels. Increasing the radiative heat flux enhances the fluid temperature, which, in turn, causes the velocity and concentration near the porous surface to rise.

The Lie symmetry group approach has been applied by several researchers to investigate countless convective boundary problems under several flow patterns in aerodynamics, plasma physics, meteorology, fluid mechanics, chemical engineering, and various other branches of engineering. It is a scaling symmetry group used to reduce two independent variables of the model to a single variable. Several papers on Lie symmetry group approach have been published which include Ahmad *et al*. [21], Das *et al*. [22], Rashidi *et al*. [23], Kandasamy *et al*. [24] and so on.

Here, our primary objective is to build upon the work of Ahmad *et al*. [21] by incorporating nonlinear thermal radiation into the energy equation, considering the effects of Soret and Dufour. This will allow us to investigate the mass and energy flux, as well as the convective Maxwell nanofluid flow, on a stretching porous sheet.

2. Mathematical Analyses

The characteristics of Soret and Dufour effects in convective Maxwell nanofluid flow on a stretching porous parallel plate with nonlinear thermal radiation are examined. The nanofluid flow, driven by thermophoresis and Brownian motion, is influenced by a magnetic field B_0. According to Figure 1, The Maxwell nanofluid is presumed to flow along the x-direction. The Boussinesq approximation is considered, and the flow is fully developed and laminar.

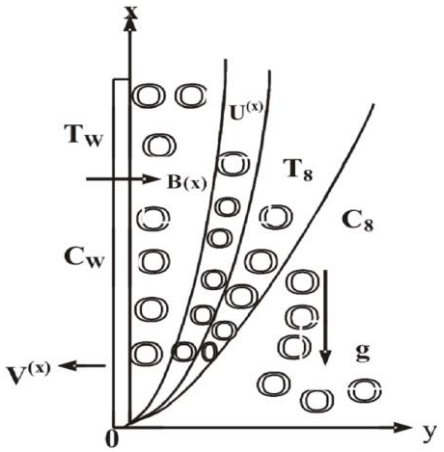

Figure 1. *The physical channel of the parallel porous plate.*

The governing expressions that drive the flow are as Ahmad *et al*. [21] and Li *et al*. [25].

$$\frac{\partial \hat{u}}{\partial \hat{x}} + \frac{\partial \hat{v}}{\partial \hat{y}} = 0 \tag{1}$$

$$\hat{u}\frac{\partial \hat{u}}{\partial \hat{x}} + \hat{v}\frac{\partial \hat{u}}{\partial \hat{y}} + \lambda\left[\hat{u}^2\frac{\partial^2 \hat{u}}{\partial \hat{x}^2} + \hat{v}^2\frac{\partial^2 \hat{u}}{\partial \hat{y}^2} + 2\hat{u}\hat{v}\frac{\partial^2 \hat{u}}{\partial \hat{x}\partial \hat{y}}\right] = \nu\frac{\partial^2 \hat{u}}{\partial \hat{y}^2} + \left[\left(1-\hat{C}_\infty\right)\rho_{f_\infty}\beta\left(\hat{T}-\hat{T}_\infty\right) - \left(\rho_p - \rho_{f_\infty}\right)\left(\hat{C}-\hat{C}_\infty\right)\right]g - \left[\frac{\sigma {B_0}^2(x)}{\rho} + \frac{v_\infty}{bk}\right]\left[\hat{u} + \lambda\hat{v}\frac{\partial \hat{u}}{\partial \hat{y}}\right] \tag{2}$$

$$\hat{u}\frac{\partial \hat{T}}{\partial \hat{x}} + \hat{v}\frac{\partial \hat{T}}{\partial \hat{y}} = \frac{\kappa}{\rho C_p}\frac{\partial^2 \hat{T}}{\partial \hat{y}^2} - \frac{1}{\rho C_p}\frac{\partial q_r}{\partial \hat{y}} + \frac{Q_0}{\rho C_p}\left(\hat{T}-\hat{T}_\infty\right) + \tau\left[D_B\frac{\partial \hat{C}}{\partial \hat{y}}\frac{\partial \hat{T}}{\partial \hat{y}} + \frac{D_T}{T_\infty}\left(\frac{\partial \hat{T}}{\partial \hat{y}}\right)^2\right] + \frac{D_B k_T\left(\hat{C}-\hat{C}_\infty\right)}{\nu C_S C_p\left(\hat{T}-\hat{T}_\infty\right)}\frac{\partial^2 \hat{C}}{\partial \hat{y}^2} \tag{3}$$

$$\hat{u}\frac{\partial \hat{C}}{\partial \hat{x}} + \nu\frac{\partial \hat{C}}{\partial \hat{y}} = D_B\frac{\partial^2 \hat{C}}{\partial \hat{y}^2} + \frac{D_T}{\hat{T}_\infty}\frac{D_B k_1\left(\hat{T}-\hat{T}_\infty\right)}{T_W\left(\hat{C}-\hat{C}_\infty\right)}\frac{\partial^2 \hat{T}}{\partial \hat{y}^2} - R\left(\hat{C}-\hat{C}_\infty\right) \tag{4}$$

The above modals boundary conditions are as Ahmed *et al*. [21]:

$$\left.\begin{aligned} &\hat{u} = \hat{U}_w(x) = C_1\hat{x}\hat{v} = \hat{v}_w(x), \hat{T} = \frac{-k\partial \hat{T}}{\partial \hat{y}} = hf\left(\hat{T}_f - \hat{T}\right), \hat{C} = \hat{C}_w at\hat{y} = 0 \\ &\hat{u} \to 0, \hat{T} \to \hat{T}_\infty, \hat{C} \to \hat{C}_\infty as\hat{y} \to \infty \end{aligned}\right\} \tag{5}$$

Below is the introduction of non- dimensional variables to dimensionless equations (1) to (5)

$$\left.\begin{aligned} &\theta = \frac{\hat{T}-\hat{T}_\infty}{\hat{T}_w-\hat{T}_\infty}, \phi = \frac{\hat{C}-\hat{C}_\infty}{\hat{C}_w-\hat{C}_\infty}, \Pr = \frac{\mu\rho c_p}{\kappa}, M = \frac{\sigma B_0^2}{\rho C_1}, Ra = \frac{\left(1-\phi_\infty\right)\beta g\Delta\theta}{V}, \\ &Le = \frac{\alpha}{D_b}, Nr = \frac{\left(\rho_p - \rho_{f_\infty}\right)\Delta\phi}{\rho_{f_\infty}\beta\Delta\theta\left(1-\phi_\infty\right)}, Nb = \frac{D_B\Delta\phi(\rho c)_p}{\kappa}, Nt = \frac{D_T\Delta\theta(\rho c)_p}{\kappa T_\infty}, K = \frac{v_\infty}{bk}, \\ &N = \frac{4T_\infty^3\sigma_1}{\mathrm{K}_1\kappa}, \gamma = \frac{Uk}{D_B}, \beta = \lambda C_1, Q = \frac{Q_0}{\rho c_p}, x = \frac{C_1}{U_1}\hat{x}, y = \sqrt{\frac{C_1}{\nu}}\hat{y}, u = \frac{\hat{u}}{U_1}, Sr = \frac{D_B k_1\left(\hat{T}-\hat{T}_\infty\right)}{T_w\left(\hat{C}-\hat{C}_\infty\right)} \\ &Df = \frac{D_B k_T\left(\hat{C}-\hat{C}_\infty\right)}{\nu c_s c_p\left(\hat{T}-\hat{T}_\infty\right)}, C_T = \frac{\hat{T}}{\hat{T}_\infty - \hat{T}} \end{aligned}\right\} \tag{6}$$

Rosseland approximation is used to simplify the radiative heat flux as follows:

$$q_r = -\frac{4\sigma_1}{3k_1}\frac{\partial T^4}{\partial y} \tag{7}$$

Expand T^4 into Taylor's series expansion In order to linearize equation (7) gives

$$T^4 = \left(\theta\left(T_1 - T_0\right) + T_0\right)^4 \tag{8}$$

By putting equations (6) to (8) into equations (1) to (5) the dimensionless equations below emerged

$$\frac{\partial u}{\partial x} + \frac{\partial v}{\partial y} = 0 \tag{9}$$

$$u\frac{\partial u}{\partial x} + v\frac{\partial u}{\partial y} + \lambda\left[u^2\frac{\partial^2 u}{\partial x^2} + v^2\frac{\partial^2 u}{\partial y^2} + 2uv\frac{\partial^2 u}{\partial x \partial y}\right] = \nu\frac{\partial^2 u}{\partial y^2} + Ra\left[\theta - N_r\phi\right] - \left[M + \frac{1}{K}\right]\left[u + \lambda v\frac{\partial u}{\partial y}\right] \tag{10}$$

$$\Pr\left[u\frac{\partial \theta}{\partial x} + v\frac{\partial \theta}{\partial y}\right] = \left[1 + \frac{4N}{3}\left(C_T + \theta\right)^3\right]\frac{\partial^2 \theta}{\partial y^2} + 4N\left[C_T + \theta\right]^2\left(\frac{\partial \theta}{\partial y}\right)^2 + Q\theta + N_b\frac{\partial \phi}{\partial y}\frac{\partial \theta}{\partial y} + N_t\left(\frac{\partial \theta}{\partial y}\right)^2 + Du\frac{\partial^2 \phi}{\partial y^2} \tag{11}$$

$$Le\left[u\frac{\partial \phi}{\partial x} + v\frac{\partial \phi}{\partial y}\right] = D_B\frac{\partial^2 \phi}{\partial y^2} + \frac{N_t}{N_b}Sr\frac{\partial^2 \theta}{\partial y^2} - \gamma\phi \tag{12}$$

The fresh boundary conditions are:

$$\left.\begin{array}{l} u = x, v = \dfrac{v_w}{\sqrt{C_1 \nu}}, \theta' = -Bi\left(1 - \theta\right), \phi = 1, aty = 0 \\ u \to 0, \theta \to 0, \phi \to 0, asy \to \infty \end{array}\right\} \tag{13}$$

Introducing the stream function defined by

$$u = \frac{\partial \psi}{\partial y}, and v = -\frac{\partial \psi}{\partial x} \tag{14}$$

The following are obtained by putting equation (14) into equations (9) to (13). Equation (9) is satisfied identically.

$$\left[\frac{\partial \psi}{\partial y}\frac{\partial^2 \psi}{\partial x \partial y} - \frac{\partial \psi}{\partial x}\frac{\partial^2 \psi}{\partial y^2}\right] + \beta\left[\left(\frac{\partial \psi}{\partial y}\right)^2\frac{\partial^3 \psi}{\partial x^2 \partial y} + \left(\frac{\partial \psi}{\partial x}\right)^2\frac{\partial^3 \psi}{\partial y^3} - 2\frac{\partial \psi}{\partial y}\frac{\partial \psi}{\partial x}\frac{\partial^3 \psi}{\partial x \partial y^2}\right] = \frac{\partial^3 \psi}{\partial y^3} + Ra\left[\theta - N_r\phi\right] - \left[M + \frac{1}{K}\right]\left(\frac{\partial \psi}{\partial y} - \beta\frac{\partial \psi}{\partial x}\frac{\partial^2 \psi}{\partial y^2}\right) \tag{15}$$

$$\Pr\left[\frac{\partial \psi}{\partial y}\frac{\partial \theta}{\partial x} - \frac{\partial \psi}{\partial x}\frac{\partial \theta}{\partial y}\right] = \left[1 + \frac{4N}{3}\left(C_T + \theta\right)^3\right]\frac{\partial^2 \theta}{\partial y^2} + 4N\left[C_T + \theta\right]^2\left(\frac{\partial \theta}{\partial y}\right)^2 + Q\theta + N_b\frac{\partial \phi}{\partial y}\frac{\partial \theta}{\partial y} + N_t\left(\frac{\partial \theta}{\partial y}\right)^2 + Du\frac{\partial^2 \phi}{\partial y^2} \tag{16}$$

$$Le\left[\frac{\partial \psi}{\partial y}\frac{\partial \phi}{\partial x} - \frac{\partial \psi}{\partial x}\frac{\partial \phi}{\partial y}\right] = \frac{\partial^2 \phi}{\partial y^2} + \frac{N_t}{N_b}Sr\frac{\partial^2 \theta}{\partial y^2} - \gamma\phi \tag{17}$$

With boundary conditions as:

$$\left.\begin{aligned} &\frac{\partial \psi}{\partial y}=x,\ \frac{\partial \psi}{\partial x}=\frac{-V_w}{\sqrt{C_1 v}},\quad \theta'=-B_i\left(1-\theta\right),\quad \phi=1 \quad at \quad y=0 \\ &\frac{\partial \psi}{\partial y}\to 0,\quad \theta\to 0,\quad \phi\to 0 \quad \text{at} \quad y\to\infty \end{aligned}\right] \tag{18}$$

2.1. Lie Group Alteration

The scaling symmetry group techniques are introduced below as Ahmed *et al*. [21]

$$\Gamma: x^*=xe^{\varepsilon\alpha_1}, y^*=ye^{\varepsilon\alpha_2}, \psi^*=\psi e^{\varepsilon\alpha_3}, \theta^*=\theta e^{\varepsilon\alpha_4}, \phi^*=\phi e^{\varepsilon\alpha_5} \tag{19}$$

By applying equation (19) into equations (15) to (18) where α is the real number and ε is the parameter of the group we got:

$$\begin{aligned} &e^{\varepsilon\left(2\alpha_2+\alpha_1-2\alpha_3\right)}\left[\frac{\partial\psi^*}{\partial y^*}\frac{\partial^2\psi^*}{\partial x^*\partial y^*}-\frac{\partial\psi^*}{\partial x^*}\frac{\partial^2\psi^*}{\partial y^{*2}}\right]+ \\ &\beta e^{\varepsilon\left(2\alpha_1+3\alpha_2-3\alpha_3\right)}\left[\left(\frac{\partial\psi^*}{\partial y^*}\right)^2\frac{\partial^3\psi^*}{\partial x^{*2}\partial y^*}+\left(\frac{\partial\psi^*}{\partial x^*}\right)^2\frac{\partial^3\psi^*}{\partial y^{*3}}-2\frac{\partial\psi^*}{\partial y^*}\frac{\partial\psi^*}{\partial x^*}\frac{\partial^3\psi^*}{\partial x^*\partial y^{*2}}\right] \\ &=e^{\varepsilon\left(3\alpha_2-\alpha_3\right)}\frac{\partial^3\psi^*}{\partial y^{*3}}+e^{-\varepsilon\alpha_4}\left[Ra\theta^*\right]-e^{-\varepsilon\alpha_5}\left[RaN_r\phi^*\right] \\ &-\left[M+\frac{1}{K}\right]\left[e^{\varepsilon\left(\alpha_2-\alpha_3\right)}\frac{\partial\psi^*}{\partial y^*}-e^{\varepsilon\left(\alpha_1+2\alpha_2-2\alpha_3\right)}\beta\frac{\partial\psi^*}{\partial x^*}\frac{\partial^2\psi^*}{\partial y^{*2}}\right] \end{aligned} \tag{20}$$

$$\begin{aligned} &e^{\varepsilon\left(\alpha_1+\alpha_2-\alpha_3-\alpha_4\right)}\Pr\left[\frac{\partial\psi^*}{\partial y^*}\frac{\partial\theta^*}{\partial x^*}-\frac{\partial\psi^*}{\partial x^*}\frac{\partial\theta^*}{\partial y^*}\right]=e^{\varepsilon\left(2\alpha_2-4\alpha_4\right)}\left[1+\frac{4}{3}N\left(C_T-\theta^*\right)^3\right]\frac{\partial^2\theta^*}{\partial y^{*2}}+ \\ &e^{\varepsilon\left(2\alpha_2-4\alpha_4\right)}4N\left[C_T+\theta^*\right]^2\left(\frac{\partial\theta^*}{\partial y^*}\right)^2+e^{\varepsilon\left(-\alpha_4\right)}Q\theta^*+e^{\varepsilon\left(2\alpha_2-\alpha_4-\alpha_5\right)}N_b\frac{\partial\phi^*}{\partial y^*}\frac{\partial\theta^*}{\partial y^*} \\ &+e^{\varepsilon\left(2\alpha_2-2\alpha_4\right)}N_t\left(\frac{\partial\theta^*}{\partial y^*}\right)^2+e^{\varepsilon\left(2\alpha_2-\alpha_5\right)}Du\frac{\partial^2\phi^*}{\partial y^{*2}} \end{aligned} \tag{21}$$

$$\begin{aligned} &e^{\varepsilon\left(\alpha_1+\alpha_2-\alpha_3-\alpha_5\right)}Le\left[\frac{\partial\psi^*}{\partial y^*}\frac{\partial\phi^*}{\partial x^*}-\frac{\partial\psi^*}{\partial x^*}\frac{\partial\phi^*}{\partial y^*}\right]=e^{\varepsilon\left(2\alpha_2-\alpha_5\right)}\frac{\partial^2\phi^*}{\partial y^{*2}} \\ &+e^{\varepsilon\left(2\alpha_2-\alpha_4\right)}\frac{N_t}{N_b}Sr\frac{\partial^2\theta^*}{\partial y^{*2}}-e^{-\varepsilon\left(\alpha_5\right)}\gamma\phi^* \end{aligned} \tag{22}$$

By equating the powers of e the invariant of the technique established for equations (20) - (22)

$$\left.\begin{array}{l}\left.\begin{array}{l}2\alpha_2+\alpha_1-2\alpha_3=2\alpha_1+3\alpha_2-3\alpha_3=3\alpha_2-\alpha_3=\\ -\alpha_4=-\alpha_5=\alpha_2-\alpha_3=\alpha_1+2\alpha_2-2\alpha_3\end{array}\right\}\\ \left.\begin{array}{l}\alpha_1+\alpha_2-\alpha_3-\alpha_4=2\alpha_2-4\alpha_4=2\alpha_2-4\alpha_4=\\ -\alpha_4=2\alpha_2-\alpha_4-\alpha_5=2\alpha_2-2\alpha_4=2\alpha_2-\alpha_5\end{array}\right\}\\ \left.\alpha_1+\alpha_2-\alpha_3-\alpha_5=2\alpha_2-\alpha_5=2\alpha_2-\alpha_4=-\alpha_5\right\}\end{array}\right\} \quad (23)$$

From equation (18), the invariance of the boundary conditions becomes:

$$\alpha_1=\alpha_3,\quad \alpha_2=\alpha_4=\alpha_5=0 \quad (24)$$

Center on the outcomes of equation (23) put on equation (24) the group alterations (19) becomes:

$$\left.\Gamma: x^*=xe^{\varepsilon\alpha_1}, y^*=y, \psi^*=\psi e^{\varepsilon\alpha_1}, \theta^*=\theta, \phi^*=\phi\right\} \quad (25)$$

Furthermore, subject to Taylor series expansions we have:

$$\left.\begin{array}{l}x^*-x=\varepsilon x\alpha_1+0(\varepsilon^2)\\ y^*-y=0\\ \psi^*-\psi=\varepsilon\psi\alpha_1+0(\varepsilon^2)\\ \theta^*-\theta=0\\ \phi^*-\phi=0\end{array}\right\} \quad (26)$$

Since $\alpha_1\neq 0$, altering equation (26), the following developed:

$$\left.y^*-y=0, \frac{x^*-x}{x\alpha_1}=\varepsilon, \theta^*-\theta=0, \frac{\psi^*-\psi}{\psi\alpha_1}=\varepsilon, \phi^*-\phi=0\right\} \quad (27)$$

Currently, in terms of differentials equation (27) yields

$$\frac{dx^*}{x^*\alpha_1}=\frac{d\psi *}{\alpha_1\psi^*} \quad (28)$$

$$d\theta^*=dy^*=d\phi^*=0 \quad (29)$$

The similarity below is attained after solving equations (28) – (29)

$$\left.y^*=\eta, \psi^*=x^* f(\eta), \theta^*=\theta(\eta) and \phi^*=\phi(\eta)\right\} \quad (30)$$

Where η, is the similarity variable
By applying equation (30) into equations (15) to (18) yielded the following:

$$f'''+\left[ff''-f'^2\right]-\beta\left[f^2f'''-2fff''\right]-\left[\left(M+\frac{1}{K}\right)\left(f'-\beta ff''\right)\right]+Ra\left[\theta-N_r\phi\right]=0 \tag{31}$$

$$\left[1+\frac{4}{3}N\left(C_T+\theta\right)^3\right]\theta''+4N\left[C_T+\theta\right]^2\theta'^2+\Pr\left[f\theta'+Q\theta+N_b\phi'\theta'+N_t\theta'^2+Du\phi''\right]=0 \tag{32}$$

$$\phi''+\frac{N_t}{N_b}Sr\theta''+Le\left[f\phi'-\gamma\phi\right]=0 \tag{33}$$

While the boundary conditions reads:

$$\left.\begin{array}{l} f=S,\ f'=1,\theta'=-Bi\left(1-\theta\right),\phi=1at\eta=0 \\ f'\to 0,\theta\to 0,\phi\to 0as\eta\to\infty \end{array}\right\} \tag{34}$$

The concerned engineering physical quantities of practical interest are C_f , Nur , and Shr as defined below:

$$C_f=\frac{1}{2}\mathrm{Re}_x^{-1/2}C_f=f''(0) \tag{35}$$

$$Nur=\mathrm{Re}_x^{-1/2}Nu=-\theta'(0) \tag{36}$$

$$Shr=\mathrm{Re}_x^{-1/2}Sh=-\phi'(0) \tag{37}$$

2.2. Method of Computation

The following transformation was applied to convert equations (31) – (34) into first-order initial value problems.

$$\left(h_1,h_2,h_3,h_4,h_5,h_6,h_7,h_8,h_9,h_{10}\right)=\left(f,f',f'',f''',\theta,\theta',\theta'',\phi,\phi',\phi''\right) \tag{38}$$

$$\begin{pmatrix} h_1 \\ h_2 \\ h_3 \\ h_4 \\ h_5 \\ h_6 \\ h_7 \end{pmatrix}=\begin{pmatrix} y_2 \\ y_3 \\ \left[\frac{1}{1-\beta y_1^2}\right]\left[-2\beta y_2y_1y_3-\left[y_1y_3-y_2^2\right]+\left[\left(M+\frac{1}{K}\right)\left(y_2-\beta y_1y_3\right)\right]+Ra\left[y_4-Nry_6\right]\right] \\ y_5 \\ \frac{1}{\left[1+\frac{4}{3}N(Ct+y_4)^3\right]}\left[-4N(Ct+y_4)^2y_5^2-Pr\left(y_1y_5+Qy_4+Nby_7y_5+Nty_5^2Duy_7\right)\right] \\ y_7 \\ -\frac{Nt}{Nb}Sry_5'-Le[y_1y_7-\gamma y_6] \end{pmatrix} \tag{39}$$

The boundary conditions

$$\begin{pmatrix} y_1(0) \\ y_2(0) \\ y_5(0) \\ y_6(0) \\ y_2(\infty) \\ y_4(\infty) \\ y_6(\infty) \end{pmatrix}=\begin{pmatrix} S \\ 1 \\ -Bi\left(1-y_4\right) \\ 1 \\ 0 \\ 0 \\ 0 \end{pmatrix} \tag{40}$$

3. Validation of Results

The analysis to validate the results was conducted in Table 1, showing excellent agreement with those of Hayat *et al*. [26], Turkyilmazoglu [27] and Ahmad *et al*. [21].

Table 1. *Evaluation of results for* $f''(0)$ *when* $\beta = Ra = S = Bi = 0$ *and* $K \to \infty$, *with previous published works.*

M	Ahmad *et al*. [21]	Hayat *et al*. [26]	Turkyilmazoglu *et al*. [27]	Present results
0.0	-1.00000	-1.00000	-1.000000	-1.00000000
0.5	-1.22474	-1.22474	-1.224744	-1.22474487
1.0	-1.41421	-1.41421	-1.414213	-1.41421356

4. Results and Discussion

The result of the combine upshot of Soret and Dufore of a convective Maxwell nanofluid on a porous stretching sheet with nonlinear thermal emission is ascertained. The impact of the appropriate nondimensional flow parameters has been considered using tables and graphs. In this study, the defaulted values are:

$$\left.\begin{aligned} &\Pr = 0.71, K = 0.5, Sr = 0.5, Du = 0.1, Ra = 0.01 \\ &Ct = 0.2, N = 0.01, Q = 0.02, M = 0.5, Nb = 0.2, \\ &Nt = 0.2, Le = 0.2, \gamma = 1, Nr = 0.5, S = 0.1, Bi = 0.1 \\ &\beta = 0.2, Nr = 0.5 \end{aligned}\right\} \quad (41)$$

Unless otherwise detailed.

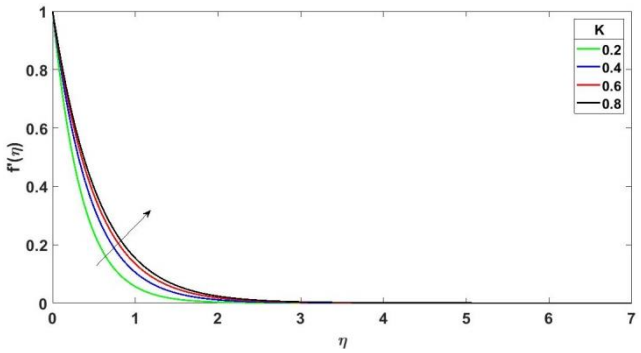

Figure 2. *Influence of* K *on* $f'(\eta)$.

Table 2. *Impact of* K *on* C_f, Nur, *and* Shr.

K	C_f	*Nur*	*Shr*
0.2	-2.77175	0.06222	0.47366
0.4	-2.17873	0.06672	0.47621
0.6	-1.94287	0.06871	0.47769

Table 3. *Impact of* Ct *on* C_f, Nur, *and Shr.*

Ct	C_f	*Nur*	*Shr*
0.2	-2.04041	0.06787	0.47704
0.7	--2.04040	0.06772	0.47723
0.9	-2.04039	0.06760	0.47739

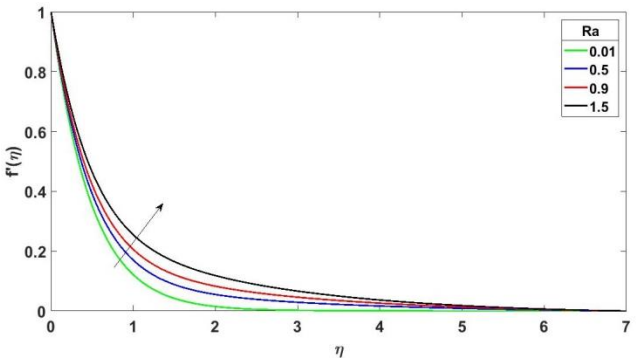

Figure 3. *Influence of* Ra *on* $f'(\eta)$.

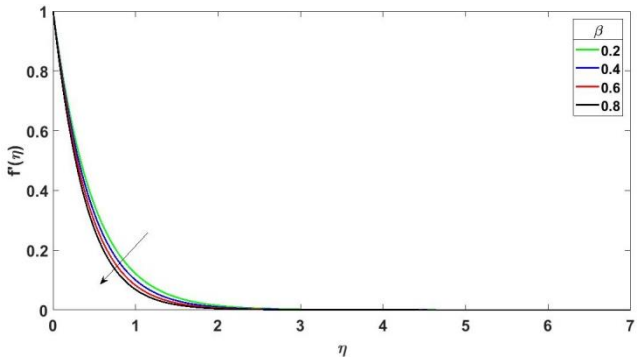

Figure 4. *Influence of* β *on* $f'(\eta)$.

However, Figure 2 examines the raising effects of K on $f'(\eta)$ outlined. This developed the momentum boundary layer as a result of K which gives interior heat to the flow

and the permeable layer becomes wide. Physically, by enhancing K the permeable hole becomes large which leads to the fast flow of fluid. Figure 3 depicts the influence of *Ra* on $f'(\eta)$ outcome. From the picture, it is clear that the $f'(\eta)$ outcome increase with rising values of *Ra* . Actually, *Ra* is the proportion of Buoyancy to the product of heat diffusion and viscous. The upshot β on $f'(\eta)$ outline is exemplified by Figure 4. By boosting the values of β consequently reduced the results of $f'(\eta)$ profile. β is used to check the fluid material and characters. Although, β is quite inconsequential if the fluid material materializes. Figure 5 explains the upshot of *S* on $f'(\eta)$ profile with growing values of *S* which in turn diminishes the $f'(\eta)$ profile. The retarding impact of *M* on $f'(\eta)$ outline is indicated in Figure 6. This physically shows that as *M* raises it magnifies the magnetic strength and it additionally upsurge the fluid particles which in turn diminishes the $f'(\eta)$.

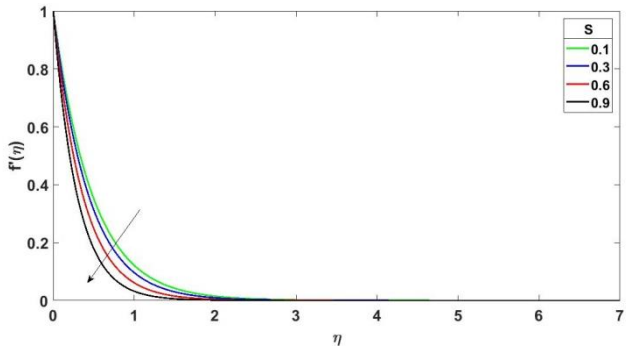

Figure 5. *Influence of* S *on* $f'(\eta)$.

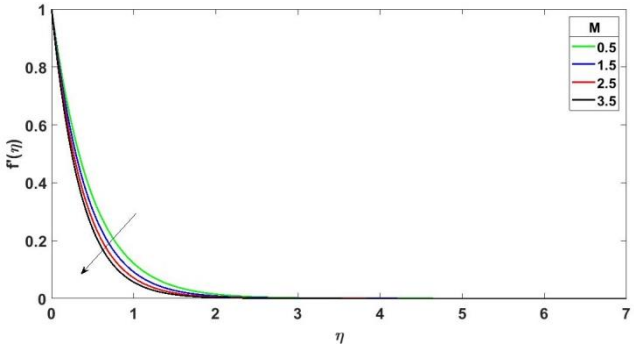

Figure 6. *Influence of* M *on* $f'(\eta)$.

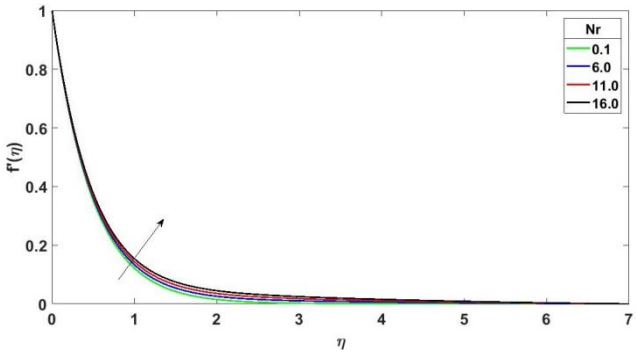

Figure 7. *Influence of* Nr *on* $f'(\eta)$.

Table 4. *Impact of* Sr *on* C_f, Nur *, and* Shr .

Sr	C_f	*Nur*	*Shr*
0.2	-2.04041	0.06766	0.48656
0.6	-2.04040	0.06794	0.47387
0.8	-2.04040	0.06808	0.46754

Table 5. *Impact of Du on* C_f, Nur *, and* Shr .

Du	C_f	*Nur*	*Shr*
0.3	-2.03952	0.05364	0.47274
0.6	-2.03823	0.03288	0.46652
0.9	-2.03700	0.01278	0.46067

Figure 7 gives the growing impact of *Nr* on $f'(\eta)$ outline. Consequently, *Nr* upsurge the buoyance force which improves the fluid velocity. Figure 8 brings foreword the action of *Du* on $\theta(\eta)$ profile. Obviously the raising of *Du* improves the $\theta(\eta)$ outline. The improvement $\theta(\eta)$ is as results of excessive concentration gradient originate from *Du* . Also, energy transport and mass diffusion take place in higher rate in the particles which in turn boost the thickness of $\theta(\eta)$. The features of *Ct* for $\theta(\eta)$ are described in Figure 9 which exhibits raising behavior when *Ct* is augmented. This is because *Ct* measured the relatively amount of interior energy within the body. Figure 10 Shows $\theta(\eta)$ variations for Q. The upsurge of Q improves $\theta(\eta)$. Basically, $\theta(\eta)$ occurrence improved greatly as a result of the presence of Q. Figure 11 demonstrates the impact of *Sr* on $\phi(\eta)$. The upsurge of *Sr* boost $\phi(\eta)$. Thermal gradient has a great effect on *Sr* .

Actually, greater Sr produces greater thermal gradient which in turn upsurged $\phi(\eta)$. Figure 12 which exhibits de-caling behavior when Le is augmented. Actually, Sr = thermal diffusivity/ mass diffusivity. Figure 13 illustrates the effect of γ on $\phi(\eta)$. The upsurge of γ decreases $\phi(\eta)$.

Table 6. *Impact of* Nb *on* C_f, Nur, *and* Shr.

Nb	C_f	*Nur*	*Shr*
0.5	-2.04024	0.06478	0.48772
1.0	-2.03990	0.05928	0.49139
2.0	-2.03910	0.04626	0.49336

Table 7. *Impact of* γ *on* C_f, *Nur, and Shr.*

γ	C_f	*Nur*	*Shr*
1.5	-2.04041	0.06603	0.57719
2.0	-2.04042	0.06452	0.66166
4.0	-2.04039	0.05994	0.92270

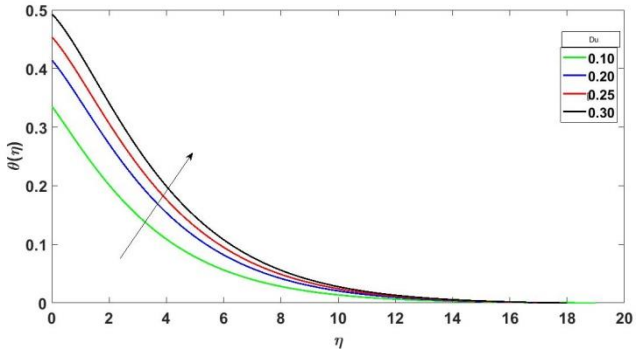

Figure 8. *Influence of* Du *on* $\theta(\eta)$.

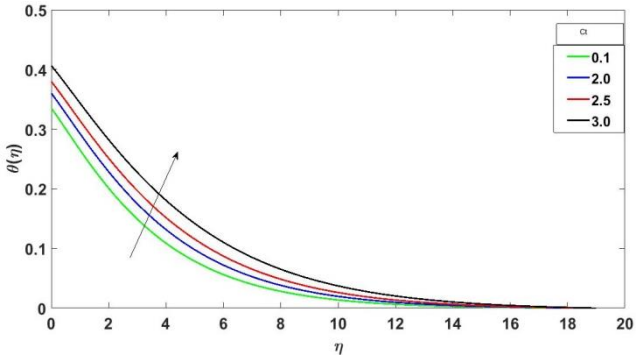

Figure 9. *Influence of* Ct *on* $\theta(\eta)$.

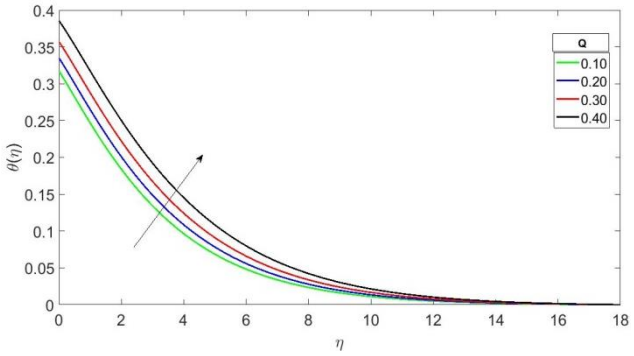

Figure 10. *Influence of* Q *on* $\theta(\eta)$.

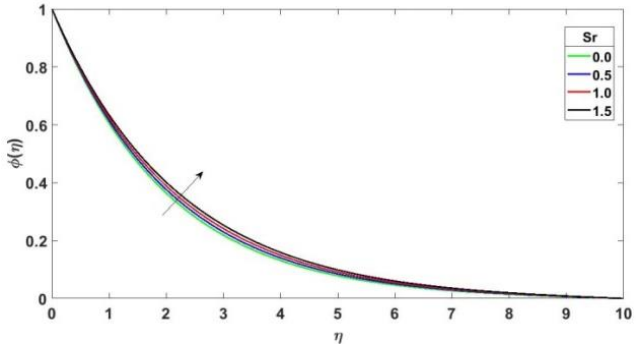

Figure 11. *Influence of* Sr *on* $\phi(\eta)$.

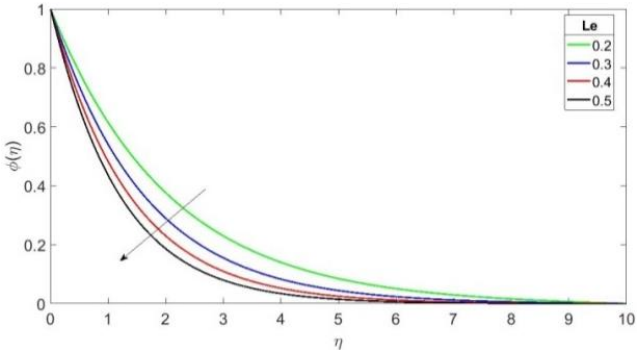

Figure 12. *Influence of* Le *on* $\phi(\eta)$.

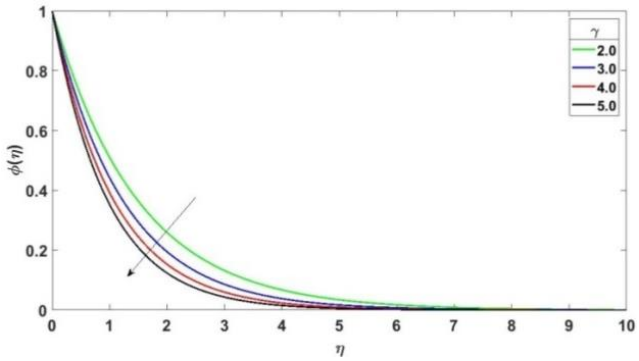

Figure 13. *Influence of* γ *on* $\phi(\eta)$.

Tables 2 to 7 were constructed to portray the effects of K, Ct, Sr, Du, Nb, γ, on C_f, Nur, and Shr. The outcomes revealed that by considering variations in values of K, Ct, Sr, Du and Nb, the magnitude C_f accelerate while it depicts reverse behavior for γ. Also, Ct, Sr and Nb declined the magnitude of Nur and inclined the magnitude with K, Du, γ. Similarly, it is experimentally perceived that rise in K, Ct, Du, Nb, and γ upsurge the Shr and decelerate with Sr.

5. Conclusion

The combined upshot of Soret and Dufore of a convective Maxwell nanofluid on a porous stretching sheet with nonlinear thermal emission was carried out. The results of the study are in form of velocity, temperature, concentration, skin friction, Nusselt number and Sherwood number. The key highlights for the present work are as follow:

i. Variations of Du and Sr outcome improves $\theta(\eta)$ and $\phi(\eta)$ respectively
ii. Both K and Du exhibits raising behavior for C_f, Nur, and Shr
iii. Both γ and Le retard the $\phi(\eta)$ outline
iv. Ct has an escalating effect on the $\theta(\eta)$ outline

Table 8. *Nomenclature.*

Symbol	Description	Symbol	Description	Symbol	Description	Symbol	Description
T_w	Reference temperature	g	Gravitational acceleration	Pr	Prandtl number	M	Hartmann number
f	Dimensionless velocity	Sr	Soret parameter	Ra	Rayleigh number	Le	Lewis number
$U(x)$	Velocity of the exterior stream	$B(x)$	Transverse magnetic field	Nr	Buoyancy ratio	Nb	Brownian motion parameter
v_∞	Condition far away from the plate	b	Constant	Nt	Thermophoresis parameter	N	Thermal radiation parameter
γ	Chemical reaction parameter	σ	Electrical conductivity	B_0	Magnetic field strength	ρ_f	Density of base fluid
ν	Kinematic viscosity	Du	Dufour parameter	u,v	Velocity components along x, y-axis	T	Temperature variable
λ	Relaxation time	η	Similarity variable	$(\rho c)_p$	Nanoparticles specific heat	C_∞	Ambient liquid concentration
ψ	Stream function	θ	Dimensionless temperature	τ	Heat capacity ratio	σ_1	Stefan-Boltzmann constant
ϕ	Dimensionless concentration	α	Thermal diffusivity	C	Nanoparticles concentration	Q_0	Non-uniform heat generation
δ	Volumetric thermal expansion coefficient of the base fluid	μ	The fluid viscosity	K^*	Mean absorption coefficient	k_1	Absorption coefficient
$(\rho c)_f$	Fluid specific heat	β	Deborah number	T_∞	Ambient liquid temperature	Q	Heat source/sink
Ct	Temperature ratio	S	Mass transfer parameter	$(\rho c)_f$	Fluid specific heat at constant pressure	Bi	Biot number
κ	Thermal conductivity	D_B	Brownian diffusion	D_T	Termophretic diffusion	C_1	Specific heat at constant pressure
K	Porous material	U	Free stream velocity of the flow	C_w	Reference concentera-tion		

Nur Nessult Number *Shr* Sherwood number

Conflicts of Interest

The authors declare no conflicts of interest.

References

[1] Ismail, F., Mohamed, B., Mohammed, H. and Abdelkhalek, A. (2020) Analytical and numerical study of Soret and Dufour effects on thermosolutal convection in a Horizontal Brinkman porous layer with a stress free upper Boundary. *Mathematical Problems in Engineering.* https://doi.org/10.1155/2020/4046570

[2] Safae, H., Abdelkhalek, A., Abdelghani, R., Hassen, B., Mohammed, H., Youssef D. and Haykel, B. (2018) Double- diffusive natural convection in an inclined enclosure with heat generation and Soret effect. *Engineering Computation* 35: (8) 2753-2774.

[3] Bidemi O. F. and Ahamed M. S. S. (2019). Soret and Dufour effects on unsteady casson magneto-nanofluid flow over an inclined plate embedded in a porous medium. *World Journal of Engineerin.* https://doi.org/10.1108/WJE-04-2018-0144

[4] Michael, W. and Isah, B. Y. (2023). On a conducting Jeffrey nanofluid flow over a stretching sheet with porous material and diffusion-thermo: a Lie group approach. *Journal of Nanosciences Research & Reports.* 5(2): 1-9.

[5] Rana, P., Srikantha, N., Muhammad, T. & Gupta, G., (2021) Computational study of three-dimensional flow and heat transfer of 25 nm Cu–H_2O nanoliquid with convective thermal condition and radiative heat flux using modified Buongiorno model. *Case Stud. Therm. Eng*. 27, 101340.

[6] Madhukesh, J. K., Ramesh, G. K., Prasannakumara, B. C., Shehzad, S. A. & Abbasi, F. M. (2021) Bio-Marangoni convection flow of Casson nanoliquid through a porous medium in the presence of chemically reactive activation energy. *Appllied Mathematics and Mechanics.* 42(8), 1191–1204.

[7] Puneeth, V., Manjunatha, S., Madhukesh, J. K. & Ramesh, G. K. (2021) Three dimensional mixed convection flow of hybrid casson nanofluid past a nonlinear stretching surface: A modified Buongiorno's model aspects. *Chaos, Solit. Fract.* 152, 111428.

[8] Khan, M. I., Qayyum, S., Hayat, T., Khan, M. I., Alsaedi, A.(2019) Entropy optimization in flow of Williamson nanofluid in the presence of chemical reaction and Joule heating, *Int. J. Heat Mass Transf*. 133: 959–967.

[9] Hayat, T., Khan, S. A., Khan, M. I., Alsaedi, A. (2019) Optimizing the theoretical analysis of entropy generation in flow of second grade nanofluid. *Phys. Scr.* 94: 085001.

[10] Gireesha, B. J., Sowmya, G., Khan, M. I., ¨Oztop, H. F.,(2019) Flow of hybrid nanofluid across a permeable longitudinal moving fin along with thermal radiation and natural convection. *Computer Methods Programs Biomedicine.* 185: 105166.

[11] Hussain, F., Subia, G. S., Nazeer, M., Ghafar, M. M., Ali, Z., Hussain, A., (2021) Simultaneous effects of Brownian motion and thermophoretic force on Eyring–Powell fluid through porous geometry. *Z. Naturforsch.* 5: https://doi.org/10.1515/zna-2021-0004

[12] Isah, B. Y., Michael, W., Mustafa, A. and Audu, A. (2023). The upshot of nonlinear thermal emission on a conducting Jeffrey nanofluid flow over a stretching sheet: a Lie group approach. *Saudi Journal of Civil Engineering*, **7**(8): 178-191.

[13] Zeid, M. A., Ali, K. K., Shaalanand, M. A., Raslan, K. R. (2019) Numerical study of thermal radiation and mass transfer effects on free convection flow over a moving vertical porous plate using cubic B-spline collocation method. *Journal of the Egyptian Mathematics Society* https://doi.org/10.1186/s42787-019-0035-8

[14] Hayat, T., Saeed, Y., Alsaedi, A., Asad, S. (2015) Effects of convective heat and mass transfer in flow of Powell-Eyring fluid past an exponentially stretching sheet. *PLoS ONE* 10 (9): e0133831.

[15] Mahanthesh, B., Gireesha, B. J., Gorla, R. S. R., (2016) Heat and mass transfer effects on the mixed convective flow of chemically reacting nanofluid past a moving/ stationary vertical plate. *Alex. Eng. J.* 55(1): 569–581.

[16] Selimefendigil, F., Coban, S. O., ¨Oztop, H. F., (2021) Numerical analysis of heat and mass transfer of a moving porous moist object in a two dimensional channel. *Int. Commun. Heat Mass Transf.* 121: 105093.

[17] Ahmed, R., Ali, N., Khan, S. U., Rashad, A. M., Nabwey, H. A., Tlili, I., (2020) Novel micro structural features on heat and mass transfer in peristaltic flow through a curved channel. *Front. Phys.* 8: 178.

[18] Khan, M., I., Waqas, M., Hayat, T., Alsaedi, A., Muhammad Imran Khan, M., I., (2017), Significance of nonlinear radiation in mixedconvection flow of magneto Walter-B nanoliquid. *International Journal of Hydrogen Energy* 42: 26408 – 26416.

[19] Ilias, M., R., Aidah Ismail N., S., Raji, N., H., A., Rawi, N., A., and Shafie, S., (2020) Unsteady aligned MHD boundary layer flow and heat transfer of a magnetic nanofluids past an inclined plate. *International Journal Mechanical Engineering.* 9(2): 197-206.

[20] Jha, B. K. and Samaila G. (2022), Nonlinear approximation for buoyancy-driven mixed convection heat and mass transfer flow over an inclined porous plate with Joule heating, nonlinear thermal radiation, viscous dissipation and thermophoresis effects. Numerical Heat Transfer, Part B: Fundamentals, https://doi.org/10.1080/10407790.2022.2150341

[21] Ahmad, B., Nawaz, A., Khan, S. U., Khan, M. I., Abbas, T., Reddy, Y. D., Guedri, K., Malik, M. Y., Goud, B. S., Galal, A. M. (2022), Thermal diffusion of Maxwell nanoparticles with diverse flow features: Lie group simulations. *International Communication in Heat and Mass Transfer.* 136: 106-164.

[22] Das, K., Sarkary, A. and Kunduz, P. K. (2017), Nanofluid Flow over a Stretching Surface in Presence of Chemical Reaction and Thermal Radiation: An Application of Lie Group Transformation. *Journal of Siberian Federal University. Mathematics & Physics.* 10(2): 146–157.

[23] Rashidi, M. M. Momoniat, E. Ferdows, M. and Basiriparsa, A. (2014), Lie group solution for free convective flow of a Nanofluid past a chemically reaction horizontal plate in a porous media *Hindawi Publishing Corporation.* http//dx.doi.org/10.1155/2014/239082

[24] Kandasamy, R., Loganathanb, P., Arasub, P. P. (2011) Scaling group transformation for MHD boundary-layer flow of a nanofluid past a vertical stretching surface in the presence of suction/injection. *Nuclear Engineering and Design* 241: 2053-2059.

[25] Li, X. Y., Mishra, S. R., Pattnaik, P. K., Baag, S., Li, M. Y., Khan, I. M., Khan, B. N., Alaoui, K. M., Khan, U. S. (2022) Numerical treatment of time dependent magnetohydrodynamic nanofluid flow of mass and heat transport subject to chemical reaction and heat source, *Alexendrial Engineering Journal.* 61: (3) 2484–2491.

[26] Hayat, T., Mustafa, M., Pop, I. (2010), Heat and mass transfer for Soret and Dufours effect on mixed convection boundary layer flow over a stretching vertical surface in a porous medium filled with a viscoelastic fluid. *Communication Nonlinear Science Numerical Simulation* 15: 1183-1196.

[27] Turkyilmazoglu, M. (2013), The analytical solution of mixed convection heat transfer and fluid flow of a MHD viscoelastic fluid over a permeable stretching surface. *International Journal mechical science.* 77: 263-268.